Elucidation of the Reaction Mechanism for High-Temperature Water Gas Shift over an Industrial-Type Copper−Chromium−Iron Oxide Catalyst

Felipe Polo-Garzon,[†] Victor Fung,[†,‡] Luan Nguyen,[§] Yu Tang,[§] Franklin Tao,[§] Yongqiang Cheng,[∥] Luke L. Daemen,[∥] Anibal J. Ramirez-Cuesta,[∥] Guo Shiou Foo,[†,∇] Minghui Zhu,[⊥,○] Israel E. Wachs,[⊥] De-en Jiang,[‡] and Zili Wu*,[†]

[†]Chemical Sciences Division and Center for Nanophase Materials Sciences, Oak Ridge National Laboratory, Oak Ridge, Tennessee 37831, United States

[‡]Department of Chemistry, University of California, Riverside, California 92521, United States

[§]Departments of Chemical Engineering and Chemistry, The University of Kansas, Lawrence, Kansas 66047, United States

[∥]Neutron Scattering Division, Oak Ridge National Laboratory, Oak Ridge, Tennessee 37831, United States

[⊥]Operando Molecular Spectroscopy & Catalysis Laboratory, Department of Chemical and Biomolecular Engineering, Lehigh University, Bethlehem, Pennsylvania 18015, United States

S *Supporting Information*

ABSTRACT: The water gas shift (WGS) reaction is of paramount importance for the chemical industry, as it constitutes, coupled with methane reforming, the main industrial route to produce hydrogen. Copper−chromium−iron oxide-based catalysts have been widely used for the high-temperature WGS reaction industrially. The WGS reaction mechanism by the $CuCrFeO_x$ catalyst has been debated for years, mainly between a "redox" mechanism involving the participation of atomic oxygen from the catalyst and an "associative" mechanism proceeding via a surface formate-like intermediate. In the present work, advanced in situ characterization techniques (infrared spectroscopy, temperature-programmed surface reaction (TPSR), near-ambient pressure XPS (NAP-XPS), and inelastic neutron scattering (INS)) were applied to determine the nature of the catalyst surface and identify surface intermediate species under WGS reaction conditions. The surface of the $CuCrFeO_x$ catalyst is found to be dynamic and becomes partially reduced under WGS reaction conditions, forming metallic Cu nanoparticles on Fe_3O_4. Neither in situ IR not INS spectroscopy detect the presence of surface formate species during WGS. TPSR experiments demonstrate that the evolution of CO_2 and H_2 from the CO/H_2O reactants follows different kinetics than the evolution of CO_2 and H_2 from HCOOH decomposition (molecule mimicking the associative mechanism). Steady-state isotopic transient kinetic analysis (SSITKA) ($CO + H_2{}^{16}O \rightarrow CO + H_2{}^{18}O$) exhibited significant $^{16}O/^{18}O$ scrambling, characteristic of a redox mechanism. Computed activation energies for elementary steps for the redox and associative mechanism by density functional theory (DFT) simulations indicate that the redox mechanism is favored over the associative mechanism. The combined spectroscopic, computational, and kinetic evidence in the present study finally resolves the WGS reaction mechanism on the industrial-type high-temperature $CuCrFeO_x$ catalyst that is shown to proceed via the redox mechanism.
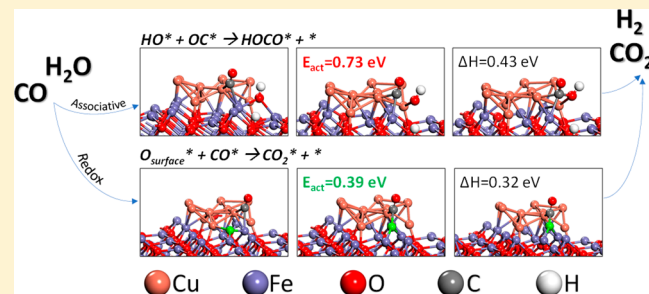
INTRODUCTION

Since its development in 1914 by Bosch and Wild,[1] the industrial water gas shift catalytic reaction (WGS) has become a paramount reaction for industrial purification of H_2 streams. Initially, the catalytic WGS reaction was used to remove CO from the H_2 stream for the Haber−Bosch ammonia synthesis,[1] and later it was used for tuning the H_2/CO ratio of syngas for production of hydrogen, methanol synthesis, and Fischer−Tropsch synthesis of hydrocarbons.[2−4] WGS is a reversible and exothermic reaction; therefore, it is thermodynamically favored

at low temperatures and kinetically favored at high temperatures.

$$CO + H_2O \leftrightarrow CO_2 + H_2 \quad \Delta H = -41 \text{ kJ/mol} \tag{1}$$

Thus, the reaction is typically performed in two stages: high-temperature WGS (HT-WGS) and low-temperature WGS (LT-WGS) . LT-WGS (~190−250 °C) is performed over copper−zinc-oxide-based catalysts, and HT-WGS (~350−450

°C) is performed over iron-oxide-based catalysts. Improving the performance of WGS catalysts is of upmost importance for hydrogen-based energy sustainability, as aimed by the United States Government.[5] Now, even more, because the dramatic increase in the production of shale gas (mostly methane) has revitalized industrial processes that involve utilization of methane, such as steam methane reforming (SMR). SMR is currently the main process for the production of H_2.[6]

The present work focuses on studying the HT-WGS catalytic reaction while presenting some comparisons to the reverse HT-WGS ($CO_2 + H_2 \leftrightarrow CO + H_2O$). For simplicity, from this point on, HT-WGS will be referred to as WGS, and reverse HT-WGS will be referred to as RWGS.

Rational design and optimization of catalysts, particularly those with industrial relevance, demand characterization of the catalysts under reaction conditions given the dynamics of catalyts with reaction environments, with the purpose of comprehending the underlying reaction mechanism. Such understanding allows targeting the rate-determining step (RDS) to enhance reaction rates. Many authors have studied the reaction mechanism for WGS. In some catalysts an "associative" mechanism has been proposed, where CO and H_2O come together to form an "associated" reaction intermediate as shown via IR (e.g., surface formate).[7] In other cases, a redox mechanism has been suggested, where CO is oxidized by surface oxygen and H_2O subsequently fills an oxygen vacancy and produces H_2.[7−9] The redox mechanism is the most commonly claimed in current reports for WGS over Fe oxide-based catalysts.[10] Recent publications have shown that, for the $CuCrFeO_x$ catalyst, chromium oxide is a textural promoter that increases the Fe_3O_4 surface area and reduces sintering. Copper, on the other hand, increases the catalytic activity over a wide range of temperature, lowers activation barriers, and, thus, increases turnover frequencies (TOF), making copper a chemical promoter.[6,11−15] TPSR studies over Cr−Fe oxide catalyst suggested a redox mechanism for the WGS reaction.[13] Although $CuCrFeO_x$ is an industrially relevant catalyst, the WGS reaction mechanism over this catalyst remains unknown, which is the focus of the present study.

In the present Article, the surface intermediates present on a $CuCrFeO_x$ catalyst are characterized under WGS reaction conditions. Kinetic measurements, near-ambient pressure X-ray photoelectron spectroscopy (NAP-XPS), infrared (IR) spectroscopy, inelastic neutron scattering (INS), and density functional theory (DFT) calculations are coupled to provide molecular level insights into the reaction mechanism. IR spectroscopy shows the surface formate intermediate is present *only* on the transient surface but is not present on the catalyst during steady-state reaction. The absence of surface formate species is supported by INS measurements on the spent catalyst. INS provides evidence for the existence of hydrides and hydroxyls on the surface. These surface intermediates were considered when describing the reaction pathway using DFT. DFT calculations showed that the redox mechanism is energetically favored over the associative mechanism. Temperature-programmed surface reaction (TPSR) experiments support this conclusion. Steady-state isotopic transient kinetic analysis (SSITKA) showed extensive scrambling of isotopic oxygen atoms, characteristic of a redox mechanism.

■ EXPERIMENTAL DETAILS

Materials. The catalyst sample ($CuCrFeO_x$) was synthesized as described previously.[16] Briefly, the catalyst was synthesized using the ammonia-assisted coprecipitation method. The precursors (iron nitrate, chromium nitrate, and copper nitrate) were mixed and dissolved in deionized water. Aqueous ammonia was added to the solution dropwise to adjust the pH to 8.5. The dark brown precipitate was aged overnight and filtered off. The filtered precipitate was dried at 80 °C for 12 h and calcined at 400 °C for 3 h in stagnant air. The fresh $CuCrFeO_x$ catalyst contains 3 wt % CuO, 8 wt % Cr_2O_3, and 89 wt % Fe_2O_3.

Argon and 5% $^{16}O_2$/He were purchased form Airgas. CO/Ar/He (2%) and 10% CO/He were purchased from Air Liquide. $H_2^{18}O$ (97 atom % ^{18}O) and formic acid (≥96%) were purchased from Sigma-Aldrich.

Near-Ambient Pressure X-ray Photoelectron Spectroscopy. In situ near-ambient pressure X-ray photoelectron spectroscopy (NAP-XPS) was performed on a lab-based system. Detailed information about the system can be found in a previous publication.[17] Briefly, the NAP-XPS system is equipped with an Al K-alpha X-ray source (SPeCS XR-MF). Photoelectrons collection was done using a differentially pumped photoelectron energy analyzer (Scienta-Omicron R4000 HIPP-2) with a 0.8 mm prelense cone aperture. Resolution of the analyzer was set at 100 eV pass energy. Heating of the sample was done using an IR laser irradiating the back of the sample holder. Sample temperature was monitored using a K-type thermocouple spot-welded on the sample holder. Reaction gases were introduced into the reaction cell using all-metal leak valves.

Infrared Spectroscopy. Infrared spectroscopy measurements were performed using a Thermo Nicolet Nexus 670 FTIR spectrometer with a mercury cadmium telluride (MCT) detector. Each spectrum was recorded with 32 scans at a resolution of 4 cm^{-1}. The sample was loaded into a crucible, and the crucible was placed inside a diffuse reflectance infrared Fourier transform spectroscopy (DRIFTS) cell (Pike Technologies). The sample was initially dehydrated in situ under 0.8% O_2/(Ar + He) at 440 °C for 2 h, and in some cases, activation under WGS reaction conditions was performed. The reactant mixture for the WGS reaction was delivered to the catalyst sample using a saturator to bubble 12 mL/min of Ar through liquid water and by flowing 18 mL/min of 2% CO/(Ar + He) to deliver a CO/H_2O ratio of 1. After activation, background spectra were collected in Ar at different temperatures. Later, the reactant mixture (H_2O + CO) was reintroduced to the cell, and spectra were collected at different temperatures. Temperatures were increased stepwise, without holding at each temperature any longer than 15 min. DRIFTS spectra for formic acid desorption were collected in a similar fashion, but bubbling liquid formic acid in 30 mL of Ar instead.

Inelastic Neutron Scattering. Inelastic neutron scattering (INS) spectra were collected at the VISION beamline of the Spallation Neutron Source (SNS) at Oak Ridge National Laboratory. The catalyst sample, $CuCrFeO_x$, was first exposed to O_2 flow at 400 °C for 1 h to remove any surface contaminations and possible water species from exposure to air. It was then transferred to a Swagelok steel cell for gas loading experiments in a He glovebox. The cell was then loaded in a closed-cycle refrigerator (CCR) and cooled down to the base temperature (5 K) for background measurement. For WGS, a 1:1 ratio of CO and H_2O was loaded into the cell, and for RWGS, a 1:1 ratio of H_2 and CO_2 was loaded. The reactions were conducted at 350 °C in the closed cell. After reaction for 2 h, in some cases the sample was cooled down to 100−110 °C and evacuated for 15 min to remove weakly bonded and gas-phase moisture, while surface intermediates remained. The sample was quenched in liquid nitrogen and then cooled to 5 K before collection of any INS spectrum.

Reference INS spectra for water and formic acid were collected separately to aid the spectral interpretation. In addition, a spectrum was collected after exposing the $CuCrFeO_x$ sample to H_2 at room temperature and 3 bar for 30 min. This spectrum constitutes the
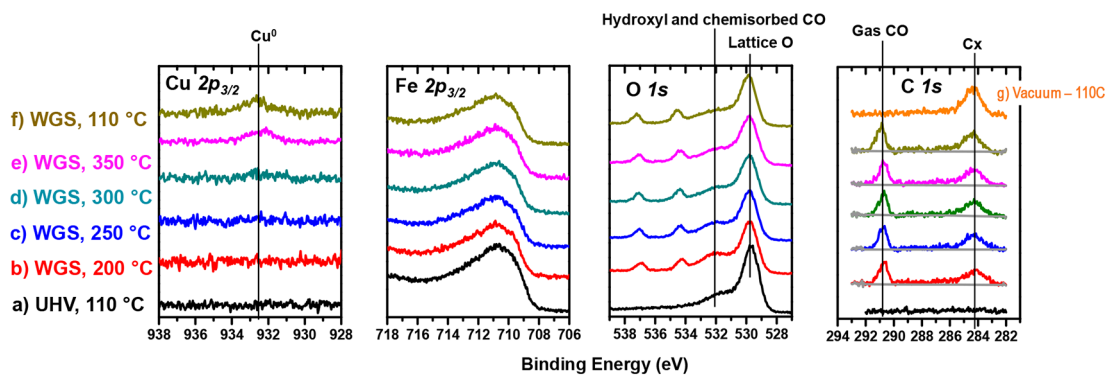
Figure 1. NAP-XPS spectra of CuCrFeO$_x$ for Cu 2p$_{3/2}$, Fe 2p$_{3/2}$, O 1s, and C 1s under (a) UHV and (b–f) under WGS reaction (0.5 Torr of CO and 0.5 Torr of H$_2$O) as the temperature was increased to (b) 200 °C, (c) 250 °C, (d) 300 °C, and (e) 350 °C and (f) decreased to 110 °C afterward. After collecting spectra under reaction conditions, a final spectrum was collected under (g) vacuum at 110 °C.

reference for the identification of hydride species. All gases were purchased from Airgas.

Density Functional Theory Calculations. All periodic density functional theory (DFT) calculations were performed with the Vienna ab initio Simulation Package (VASP).[18,19] The Perdew−Burke−Ernzerhof (PBE)[20] functional of generalized-gradient approximation (GGA) with Hubbard U correction (U = 3.8 eV)[21] was used for electron exchange and correlation. The electron−core interaction was described using the projector-augmented wave method (PAW).[22,23] A Monkhorst−Pack k-point sampling scheme[24] (3 × 3 × 1) is used. A plane wave cutoff of 400 eV is used in all calculations. Transition states were found using the climbing-image nudged elastic band (CI-NEB) method.[25] The structure modeled was spinel Fe$_3$O$_4$ with the plane (111) exposed at the surface, providing a Fe^{2+}/Fe^{3+} terminated surface. The bottom two layers of the simulated slab were fixed. A vacuum layer of 15 Å was set between slabs to minimize the interactions of the periodic images.

Temperature-Programmed Surface Reaction. Temperature-programmed surface reaction (TPSR) experiments for WGS and formic acid decomposition were performed in an Altamira Instruments system (AMI-200). The catalyst sample (20 mg) was loaded into a U-tube quartz reactor and held in place using quartz wool. Before each TSPR experiment, the catalyst sample was initially pretreated in situ at 440 °C under 50 mL/min of 5% O$_2$/He for 2 h, and subsequently under WGS reaction conditions (0.66 μL/min of H$_2$O and 50 mL/min of 1.8% CO/(Ar + He) for a H$_2$O/CO ratio of ~1) at 415 °C for at least 2 h to activate the catalyst. Liquid feeds (water or formic acid) were introduced to the reactive system using a Nexus 3000 syringe pump (Chemyx) at 50 °C, and then the catalyst was heated up to 415 °C at a ramping rate of 5 °C/min. The outlet from the reactor was analyzed using an OmniStar mass spectrometer from Pfeiffer Vacuum. The masses followed were: 2 (H$_2$), 18 (H$_2$O), 28 (CO), 29 (formic acid), and 44 (CO$_2$). The contributions from different components to a single mass were decoupled and subtracted.

Steady-State Isotopic Transient Kinetic Analysis. Steady-state isotopic transient kinetic analysis (SSITKA) experiments were performed in a home-built system equipped with back-pressure regulators and digital pressure readers to ensure the pressure inside the reactor is constant during the isotopic switch at 1.7 atm. The temperature in the lines was held at least at 120 °C to avoid condensation of components. This home-built system was coupled to the furnace of an AMI-200 unit (Altamira Instruments, Inc.) to only control the temperature inside the bed. Inside the furnace, a U-tube quartz reactor was placed containing 20 mg of the catalyst. The catalyst was held in place using quartz wool (see Scheme S1 for the SSITKA setup).

Before the isotopic switch, the catalyst sample was pretreated in situ at 410 °C under 50 mL/min of 5% O$_2$/He for 2 h, and under WGS reaction conditions (2 μL/min H$_2$O, 16.5 mL/min 10% CO/He, and 33.5 mL/min 2%Ar/He) at 410 °C for at least 2 h to activate the catalyst and achieve steady-state conditions. The isotopic switch,

H$_2^{16}$O ↔ H$_2^{18}$O, was possible using two Nexus 3000 syringe pumps from Chemyx. An OmniStar mass spectrometer from Pfeiffer Vacuum was used to analyze the outlet from the reactor. The masses followed during the switch were: 2 (H$_2$), 4 (He), 17 (H$_2$O), 19 (H$_2^{18}$O), 22 (Ne), 28 (CO), 30 (C^{18}O), 40 (Ar), 44 (CO$_2$), 46 (C^{16}O^{18}O), and 48 (C^{18}O$_2$). These masses were selected to avoid overlap of signals as much as possible; when the overlap of signals was unavoidable, proper decoupling of contributions from each component was carried out.

RESULTS AND DISCUSSION

In Situ NAP-XPS. NAP-XPS measurements were conducted to obtain information on the surface composition and oxidation states of the catalyst components and surface species under WGS reaction conditions (Figure 1). The fresh sample was initially analyzed in UHV at 110 °C; then, it was exposed to a mixture of CO and H$_2$O (1:1). The temperature was increased stepwise from 200 to 350 °C, and spectra were collected at each temperature. Later, the sample was cooled down in CO + H$_2$O to 110 °C, and a spectrum was collected; this was followed by a spectrum under vacuum at the same temperature. The sample was held at each temperature for at least 20 min (2 h at 350 °C) before data were collected.

As observed in Figure 1e and f, a signal for Cu^0 (~932.5 eV) is detected at the usual reaction temperature (~350 °C) and it remains after cooling down the system to 110 °C (Figure 1f), which is evidence of the formation of metallic copper at the surface. The formation of metallic Cu nanoparticles at the surface under reaction conditions, the product of surface enrichment from Cu cations initially dispersed in the bulk, has been previously observed.[16,26,27] An overlayer of an FeO$_x$-shell on metallic Cu nanoparticles has also been previously detected due to the so-called strong metal−support interaction (SMSI) between reducible oxides and metals.[16,28]

Partial reduction of the surface iron oxide from Fe$_2$O$_3$ to Fe$_3$O$_4$ is characterized by the disappearance of a peak at 719 eV from Fe$_2$O$_3$ and a slight broadening of the peak at ~708 eV.[16] The NAP-XPS data collected for Fe 2p$_{3/2}$ (Figure 1) did not cover binding energies out to 719 eV, and it is hard to distinguish broadening at 708 eV. However, a previous study shows that iron in the CuCrFeO$_x$ catalyst reduces to Fe$_3$O$_4$ under WGS reaction conditions.[16] Under RWGS at 350 °C, the reduction of Fe$_2$O$_3$ to Fe$_3$O$_4$ during RWGS at 350 °C was confirmed via NAP-XPS experiments (Figure S1b). The peak at 719 eV for the dehydrated Fe$_2$O$_3$ sample (treated under O$_2$ at 400 °C) disappears as soon as the RWGS mixture is introduced at 350 °C, confirming the transition to Fe$_3$O$_4$. On
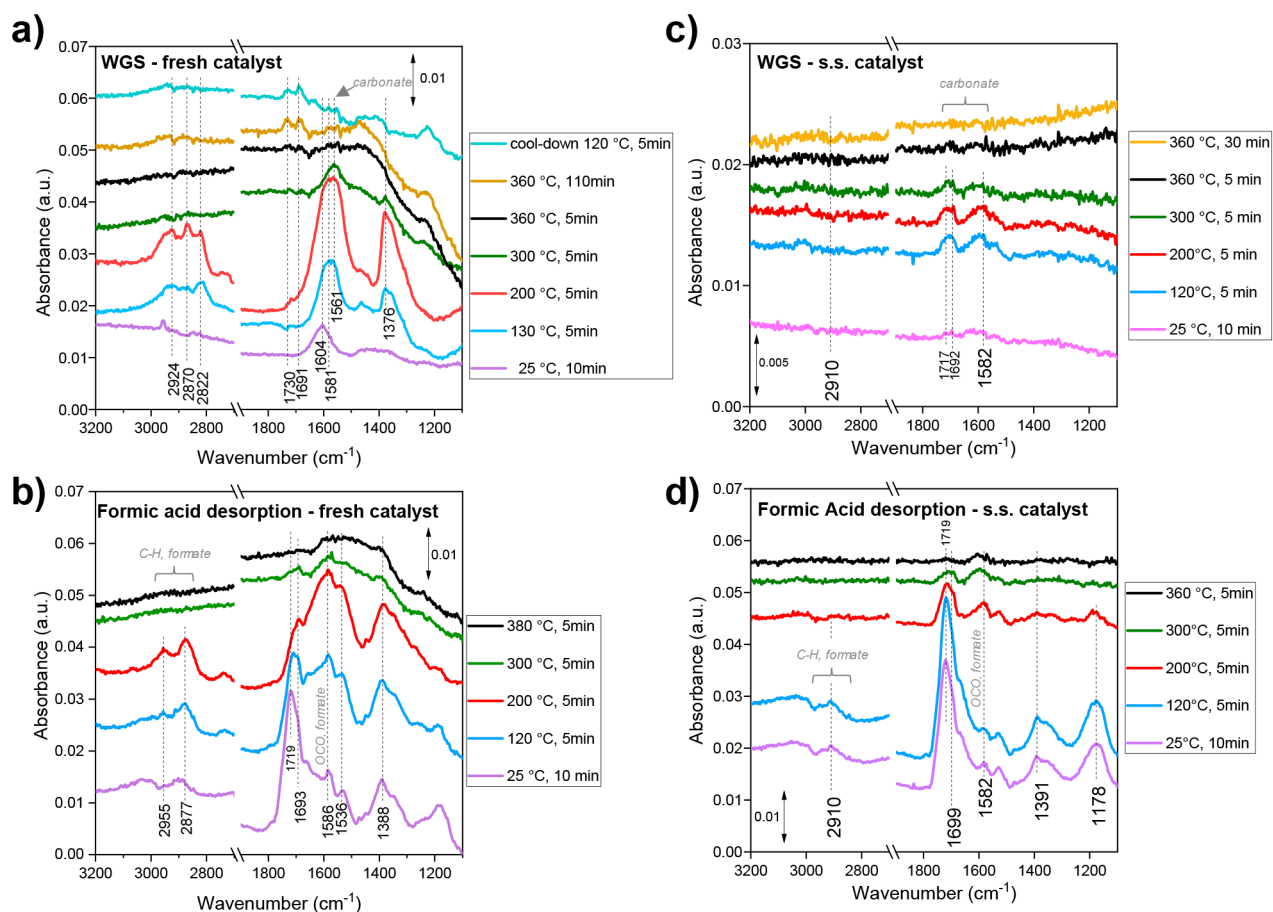
Figure 2. In situ DRIFTS study of adsorbed species on a fresh $CuCrFeO_x$ catalyst (a) under WGS gas mixture and (b) after formic acid desorption. In situ DRIFTS study of adsorbed species on a reconstructed (activated under WGS reaction conditions at 364 °C for 1 h) $CuCrFeO_x$ catalyst (c) under WGS gas mixture and (d) after formic acid desorption.

the basis of data in the present Article for the reduction of iron oxide in $CuCrFeO_x$ under RWGS (Figure S1b) and previously reported data on the same reduction under WGS,[16] we assume that the sample under study in the present Article also reduces from Fe_2O_3 to Fe_3O_4 under WGS reaction conditions. Further, the present sample and the one used in the literature were synthesized following the same procedure.[16] From Figure 1, a weak signal for hydroxyl and/or chemisorbed CO is observed at ~532 eV along with surface carbonaceous deposits (C_xH_y, 284.4 eV) and gas-phase CO (~291 eV).[29] The surface carbon is considered a spectator because the relative signal does not change as the reaction temperature is increased. Notably, surface formate species were not observed under reaction conditions, with an expected binding energy of 288−289 eV in the C 1s region.[29]

Similar NAP-XPS experiments were performed under RWGS reaction conditions (Figure S1). Evidence of surface intermediates in the C 1s region is observed, but the poor signal-to-noise ratio and the broadness of the peak (288−290 eV) make it nearly impossible to identify these species. Some possible candidates would be surface HCOO, HOCO, CO_3, or $CO_2^{-\delta}$ species.[29]

The NAP-XPS results clearly show that the catalyst under reaction conditions is significantly different when compared with the fresh catalyst (formation of metallic Cu and Fe_3O_4, surface carbonaceous deposits, and surface intermediates); therefore, any relevant characterization must be performed

under in situ/operando reaction conditions. The Fe_3O_4 crystal structure will also be used for the DFT calculations presented later in this Article.

In Situ IR Spectroscopy. Initially, the surface species on the transient $CuCrFeO_x$ catalyst (before reaching steady-state reconstruction), after *only* O_2 treatment at 440 °C for 2 h, were probed via IR spectroscopy both under WGS (Figure 2a) and during formic acid desorption (Figure 2b). On the transient catalyst, surface formate species, characterized by the OCO mode at ~1586 cm^{-1} and the C−H vibrational modes ~3000 cm^{-1} (Figure 2b),[30−33] are observed under the WGS reactant mixture (Figure 2a) up to 200 °C, although the WGS products are not generated at such low temperatures as shown later via TPSR experiments. At 300 °C, the features of surface formate due to formic acid adsorption/desorption are barely distinguishable (Figure 2b); therefore, we propose that the peak at 1561 cm^{-1} under 300 °C WGS reaction conditions (Figure 2a) is due to surface carbonates. The evident change in the baseline of the spectra under WGS at normal operating temperatures (300−360 °C) is due to the reconstruction of the surface. In the spectra for fomic acid desorption (Figure 2b), the modes between 1388 and 1719 cm^{-1}, other than 1586 cm^{-1}, are assigned to molecularly adsorbed formic acid.

To compare the surface species under steady-state WGS reaction conditions, the $CuCrFeO_x$ catalyst was pretreated under O_2 at 440 °C for 2 h, followed by exposure to CO + H_2O at 364 °C for 1 h, before recording IR spectra under

WGS reaction conditions (Figure 2c). Assignment of IR modes corresponding to surface formate species on the steady-state sample (after pretreatment under WGS at 364 °C) was done through adsorption (and subsequent desorption) of formic acid (see Figure 2d). The presence of surface formate-like species based on the C−H vibrational mode (∼2910 cm^{-1}) was not observed under WGS over the whole temperature range. The characteristic OCO mode of surface formate species (1582 cm^{-1}) was not clearly evident, and the broad band in this vicinity is rather presumed to be due to surface carbonates, along with bands at 1692 and 1717 cm^{-1}.

A very important observation is that, for the catalyst conditioned under steady-state WGS reaction (see Figure 2d), the bands for molecularly adsorbed formic acid (1719, 1392, and 1178 cm^{-1}) are more prominent than the band from the OCO mode for surface formate species (1582 cm^{-1}). This is opposite to the observation for the fresh catalyst (Figure 2b) and suggests that formic acid dissociation into surface formate proceeds easier on the fresh (transient) catalyst surface.

A better IR signal-to-noise ratio was obtained for the transient catalyst (Figure 2a and b) compared to the steady-state catalyst (Figure 2c and d), which is probably due to the presence of surface carbon deposits as indicated by NAP-XPS data in Figure 1 and reduction of the surface that significantly decreased sample reflectance.

From the in situ IR studies, it is concluded that surface formate species are present on the transient catalyst up to 200 °C, but there is no conclusive evidence for the presence of surface formate species at any temperature under the steady-state WGS reaction. Thus, although surface formate readily forms on the initial oxidized surface, it has difficulty forming on the surface of the WGS-activated catalyst because of the distinctly different types of surfaces formed as presented earlier in the NAP-XPS section.

When comparing the fresh and the spent catalyst using spectroscopic techniques (NAP-XPS and IR), it is evident that the change in the catalyst structure under reaction conditions affects the formation of surface species. The extent of reconstruction of samples with other Cu loadings and particle size would have an impact on the WGS reaction mechanism only if the nature of the active sites changes (not their density). Careful investigation of related CuCrFeO$_x$ samples with different Cu loadings, Cu particle sizes, and extents of Cu-FeO$_x$ interaction is certainly of great interest, but it lies beyond the scope of the present work.

In Situ INS. Further information about the possible presence of surface formate species during WGS and RWGS over the CuCrFeO$_x$ catalyst was sought using in situ neutron spectroscopy. This is the first time INS measurements have been conducted for a catalytic WGS system, and this is one of few reports on neutron spectroscopy for metal oxide catalysts of industrial relevance.[34]

As indicated in Figure 3a, the WGS reaction was performed at 350 °C and INS spectra were collected at 5 K before and after pumping out the chamber at 100 °C. Reference spectra for water, formic acid, and hydride species were also collected and are shown in Figure 3a. The broad band for the hydride reference at 770−780 cm^{-1} is assumed to be mostly due to surface and/or bulk hydride species because the contribution of hydroxyl species is minor, given that OH modes on iron oxide have been reported in the vicinity of 933−951 and 3385−3640 cm^{-1}.[35] From Figure 3a, it is readily determined that water is removed by pumping out the chamber and that
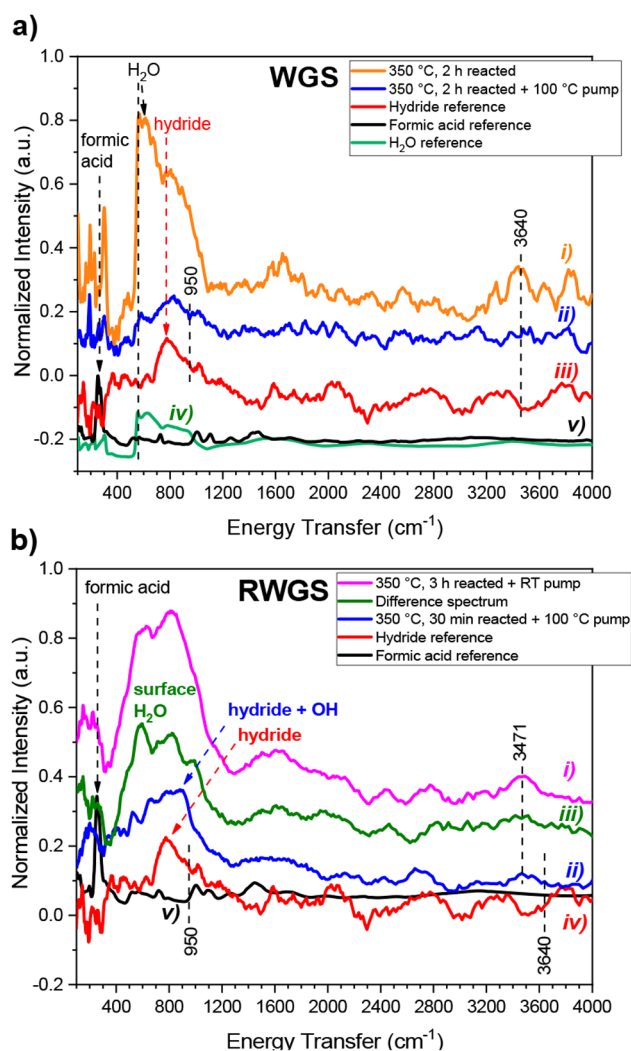
Figure 3. INS spectra collected at 5 K (a-i) after WGS reaction (CO/H$_2$O = 1) over CuCrFeO$_x$ at 350 °C for 2 h, (a-ii) after WGS reaction over CuCrFeO$_x$ at 350 °C for 2 h followed by evacuation at 100 °C, and reference spectra for (a-iii) hydride (on CuCrFeO$_x$), (a-iv) water, and (a-v) formic acid. (b-i) After RWGS reaction (CO$_2$/H$_2$ = 1) over CuCrFeO$_x$ at 350 °C for 3 h followed by evacuation at room temperature (RT), (b-ii) after RWGS over CuCrFeO$_x$ at 350 °C for 30 min followed by evacuation at 110 °C, (b-iii) difference spectrum between b-i and b-ii, and reference spectra for (b-iv) hydride (on CuCrFeO$_x$) and (b-v) formic acid.

hydride species are present on the catalyst surface. Hydroxyl species are probably also present on the surface due to the broadness of the peak centered ∼850 cm^{-1}, which might overlap with hydroxyl modes (933−951 cm^{-1}). The absence of the characteristic surface formate INS vibrational mode at 280 cm^{-1} (Figure 3a-v) after the WGS reaction (Figure 3a-ii) suggests that surface formate species are not present on the catalyst after activating the catalyst under WGS reaction conditions. The INS formic acid reference spectrum showed good agreement with simulation results, thus confirming the reliability of the characteristic peak at 280 cm^{-1} (Figures S2 and S3).

INS results after performing the RWGS reaction (Figure 3b) were similar to those recorded for WGS over CuCrFeOx. Physisorbed water was removed from the chamber after pumping at 110 °C. The difference spectrum, between the

spent catalyst before and after pumping at 110 °C, reveals the characteristics of surface water (Figure 3b-iii), which are similar to the spectrum for water collected as a reference (Figure 3a-iv). Hydride and hydroxyl species were identified on the surface of the catalyst after the RWGS. In addition, the 280 cm^{-1} band of surface formate species is absent, suggesting that it is not present after activating the catalyst under the RWGS reaction conditions. INS, however, provided insight into the presence of surface hydroxyl and hydride intermediates. *This is the first spectroscopic evidence of surface hydride after activating FeOx-based catalysts under WGS and RWGS reaction conditions.*

DFT simulations showed comparable hydrogen adsorption energies (from −3.2 to −3.5 eV) as both hydroxyl groups on Fe_3O_4 and as hydrides on the Cu−Fe interface and undercoordinated Cu edges (Figure S4). Therefore, Cu−H hydride and O−H species are expected to coexist on the surface as found with INS. The vibrational modes obtained via DFT (Figure S5) support the existence of Cu−H and Fe−OH surface species when compared to the INS spectra for surface species collected after the WGS reaction at 350 °C (Figure 3a-ii) and hydride reference (Figure 3a-iii). Bader charge for hydrogen adsorbed on Cu(111) (Figures S4a and S5) was found to be −0.263, suggesting that it can be considered a hydride as it is slightly negatively charged. Formation of Fe−H is energetically disfavored, and its vibrational mode was not detected in the experimental INS spectra.

TPSR. TPSR experiments were also performed over the $CuCrFeO_x$ catalyst, preactivated under WGS reaction conditions, to study the kinetic evolution of the products (CO_2 and H_2). Under the assumption that both CO_2 and H_2 proceed from the decomposition of a common surface intermediate (e.g., HCOO*), the kinetic evolution of CO_2 and H_2 should have the same light-off temperature and kinetic behavior.[36] Indeed, TPSR of formic acid decomposition (Figure 4a) shows a monotonic and similar evolution of CO_2 and H_2. In contrast, the evolution of CO_2 precedes the evolution of H_2 during WGS (Figure 4b).

TPSR curves from the $CuCrFeO_x$ catalyst (Figure 4a and b) exhibit a light-off temperature for H_2 at ∼135 °C for formic acid decomposition and at ∼155 °C for WGS. This indicates that the reaction mechanism for WGS over the $CuCrFeO_x$

catalyst does not proceed through a surface formate intermediate, as this intermediate decomposes at the lower temperature of ∼135 °C.

SSITKA ($H_2^{16}O + C^{16}O \leftrightarrow H_2^{18}O + C^{16}O$). To study the oxygen-exchange properties of the $CuCrFeO_x$ catalyst system under WGS reaction conditions, SSITKA experiments were undertaken. The steady-state reaction conditions under a regular reactant mixture ($C^{16}O + H_2^{16}O + Ar + He$) were achieved after 2 h at 410 °C, and then an isotopic reactant mixture was introduced ($C^{16}O + H_2^{18}O + Ne + He$). When the isotopic reactant mixture was introduced ($CO + H_2^{18}O$), multiple isotopic product species were generated: $C^{16}O_2$, $C^{16}O^{18}O$, and $C^{18}O_2$. Even, the reactants $C^{18}O$ and $H_2^{16}O$ were "generated" from the RWGS reaction (Figure S6). The generation of these species undoubtedly unveils a dynamic catalyst surface that facilitates the scrambling of $^{18}O/^{16}O$ atoms. Because the scrambling of oxygen atoms between gas-phase species and the surface is evident, the surface will arrive to a steady-state coverage of ^{18}O and ^{16}O species, given that the surface and bulk before the isotopic switch contain only ^{16}O atoms.

From the normalized responses at 410 °C (Figure 5a), it is seen that the signals of two of the isotopes of carbon dioxide ($C^{16}O_2$ and $C^{18}O_2$) plateau out only ∼45 s after the isotopic switch (note the sharp decay/increase of the Ar/Ne signal reflecting the system response). Along with $C^{16}O_2$ and $C^{18}O_2$, other species ($C^{18}O$, $H_2^{18}O$, $H_2^{16}O$, and $C^{16}O$) require a similar time to reach a steady concentration. The MS signal for $C^{16}O^{18}O$, however, reaches a steady-state value in a significantly shorter time after the isotopic switch at 410 °C (∼20 s). The time it takes for a certain species to reach a steady production rate is a convolution of the surface residence time and the time that it takes for the $^{16}O/^{18}O$ scramble process to reach steady state. It appears that the fast formation of $C^{16}O^{18}O$ reflects the high WGS reaction rate at 410 °C, and the other isotope products arise from further adsorption and oxygen scrabling. The SSITKA results point to a single concise conclusion: the intense scrambling of atoms leads to significant fractions of different isotopes, including isotopes of the reactants (Figure 5b). This behavior supports a redox mechanism.

DFT Calculations: Redox versus Associative Mechanism. DFT studies have been previously performed for WGS on the Cu(111)[37] and Fe_3O_4 surfaces.[38] On Cu(111), the associative mechanism is suggested to be dominant, with O−H cleavage of water as the rate-determining step. In contrast, the redox pathway is suggested to be dominant on Fe_3O_4, with the desorption of CO_2 as the rate-determining step.

The presence of metallic Cu nanoparticles on the surface of $CrFeO_x$ has been shown to increase the TOF value relative to bare $CrFeO_x$ (Cr has been shown to be a structural promoter, increasing surface area and stability but not the TOF).[13] In addition, it has been shown that a SMSI effect is present where FeO_x migrates onto the metallic Cu nanoparticles.[16,28] Therefore, we constructed a model system that captures the combined Cu−Fe_3O_4 active sites. A 10-atom Cu cluster was supported on the (111) surface of a Fe_3O_4 slab, to model the interaction of intermediates with the supported-metal system. This cluster is large enough to exhibit metal-like characteristics (as shown experimentally via NAP-XPS experiments, Figures 1 and S1) yet computationally affordable together with the oxide support. Distorted planar Cu(111)-like configuration was the
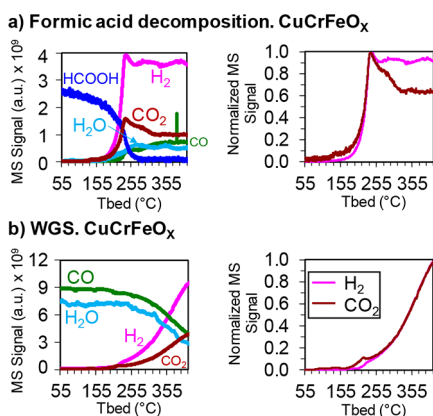
Figure 4. TPSR (5 °C/min, 20 mg of catalyst) after activation at 440 °C under 50 mL/min of 5% O_2/He for 2 h and under WGS reaction conditions ($CO/H_2O = 1$) at 415 °C for at least 2 h. (a) Formic acid decomposition over $CuCrFeO_x$ (0.45 μL/min of formic acid, 45 mL/min Ar) and (b) WGS over $CuCrFeO_x$.

a)

b)
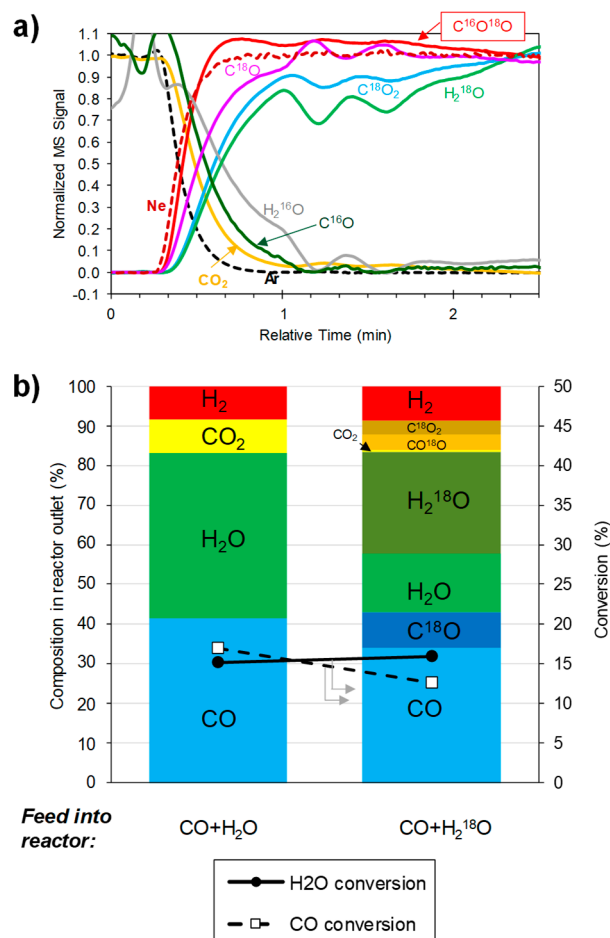
Figure 5. (a) Normalized SSITKA results for WGS over an activated CuCrFeOx sample. Regular reactant mixture: 2 μL/min H_2O, 16.5 mL/min 10% CO/He, and 33.5 mL/min 2%Ar/He. Isotopic mixture: 2 μL/min $H_2^{18}O$, 16.5 mL/min 10% CO/He, and 33.5 mL/min 2% Ne/He. Reaction conditions: 21 mg of catalyst, 1.7 atm, 410 °C. (b) Concentration of gas-phase species and conversion before and after the switch.

most energetically preferred configuration of the cluster (Figure S7).

It was found that CO adsorbs the strongest on the Cu−Fe interface (−1.60 eV; Figure 6), in agreement with the results from Xue et al.[39] The adsorption of CO on the pristine Fe_3O_4(111) surface was found to be −1.11 eV, consistent with the literature.[40] Additionally, CO adsorption on the pure Cu(111) surface is −0.94 eV,[37] which is in agreement with our results for the supported cluster, −0.8 to −1.0 eV. According
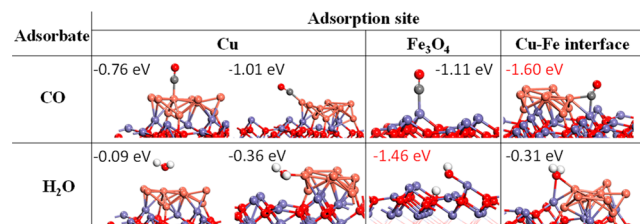
Figure 6. Adsorption configurations for CO and H_2O on different adsorption sites of the simulated Cu/Fe_3O_4 catalyst. Color code: Fe, purple; Cu, coral; O, red; C, gray; H, white.

to our results, H_2O adsorption is weak, ranging from −0.1 to −0.4 eV for Cu and Cu−Fe sites (Figure 6), in agreement with Gokhale et al.,[37] who reported weak H_2O adsorption on Cu(111) (−0.18 eV). In contrast, H_2O was found to dissociate with a negligible barrier on Fe_3O_4, again agreeing with the literature.[38] In short, the Cu−Fe interface is responsible for preferential CO adsorption, whereas water adsorbs and easily dissociates on the Fe_3O_4 support.

Next, the energetics in the reaction pathways via the associative and the redox mechanism were studied. As shown in Figure 7a, the highest barrier in the associative mechanism is 0.73 eV for the A-i step (formation of HOCO from OH and CO on the surface), while the highest barrier in the redox mechanism is 0.39 eV for the R-ii step (formation of CO_2 from O and CO on the surface). Although the enthalpy for CO_2 desorption in the redox pathway presents a high barrier (1.31 eV), the energy required for desorption reduces considerably (Gibbs free energy) after the entropy contribution at 400 °C is included. The Gibbs free energies at 400 °C for other desorption/adsorption processes were also calculated, and the results do not change the conclusion that the redox mechanism is preferred based on the DFT energetics.

In the redox mechanism, lattice oxygen can easily diffuse from the sublayer to the top layer of the catalyst (E_{act} = 0.31 eV, Figure 7b, R-i) and then undergo reaction with adsorbed CO to form adsorbed CO_2 (E_{act} = 0.39 eV, Figure 7b, R-ii), which subsequently desorbs. Following CO_2 desorption, the oxygen vacancy can be easily refilled by H_2O. H_2O first adsorbs on the Fe−Fe bridge and later dissociates with a negligible barrier (Figure 7b, R-iii). Dissociation of the surface hydroxyl species is also facile (E_{act} = 0.16 eV, not shown in Figure 7).

In the associative pathway, surface OH* and CO* can both strongly coadsorb near the Cu−Fe interface, where the HO−CO association barrier was found to be 0.73 eV (Figure 7b, A-i), comparable to 0.61 eV on Cu(111) and lower than the 1.24 eV barrier on Fe_3O_4. The O−H bond in the formed HOCO* intermediate can be readily cleaved by Cu sites in the present model with a barrier of 0.66 eV, following a facile rotation of the molecule (Figure 7b, A-ii and A-iii). Next, CO_2 desorption occurs. Although surface formate species were not directly observed in the most favorable pathway, the transition from the HOCO* species to the HCOO* species (formate) has a barrier of ∼0.92 eV (Figure S8b).

H_2 formation can occur on Cu/Fe_3O_4 through various mechanisms. One mechanism is shown in Figure S8a (E_{act} = 0.78 eV), facilitated by facile H migration between the cluster and the oxide (Figure S8b). In conclusion, DFT calculations clearly show that the favored CO adsorption at Cu−Fe sites is crucial for driving the subsequent steps in both the associative and redox pathways, with the redox mechanism favored.

■ CONCLUSIONS

The water gas shift reaction has been investigated over an industrial-type CuCrFeO$_x$ catalyst using in situ characterization, reaction kinetics, and computational tools. Efforts were devoted to discerning between the redox and associative mechanisms, with the latter characterized by the existence of an active surface "formate-like" intermediate (HCOO*, HOCO*).

In situ NAP-XPS surface analysis demonstrates that the surface of the CuCrFeO$_x$ catalyst is dynamic, with the catalyst undergoing dramatic reconstruction during WGS/RWGS reaction conditions from an initial oxidized surface to a
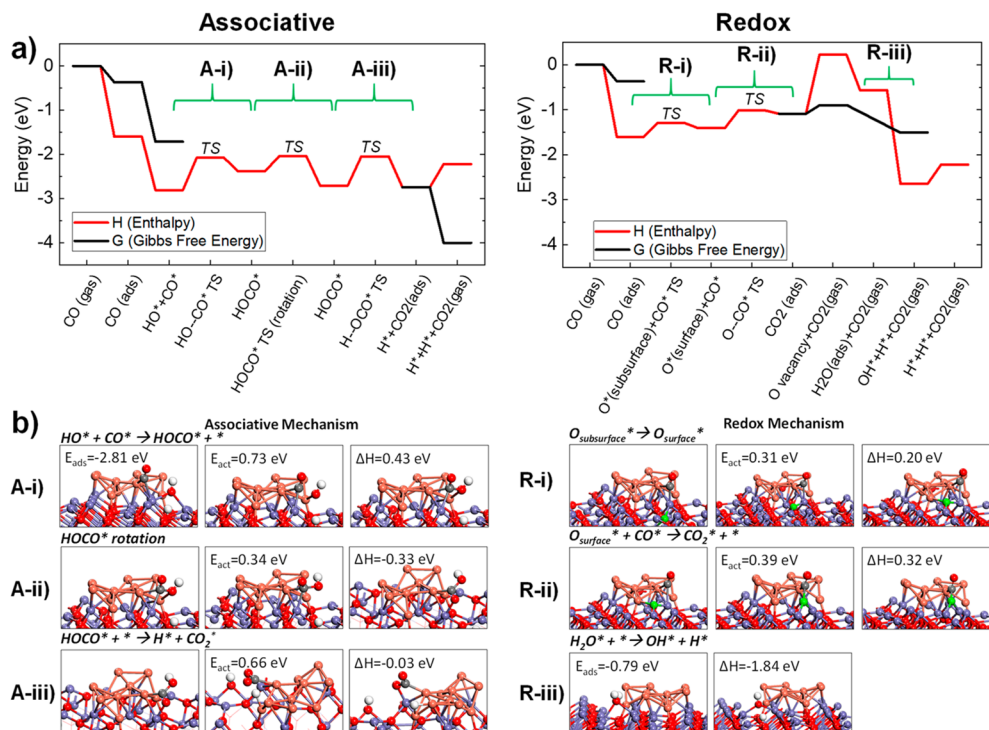
Figure 7. (a) Potential energy diagram for WGS over the simulated Cu/Fe$_3$O$_4$. (b) Structures of elementary steps involved in the associative (A-i through A-iii) and redox (R-i through R-iii) pathways. Labels (A-i, R-i, and so on) in (a) are correlated to the structures in (b). The step OH* + H* → H* + H* in the redox mechanism involves O−H dissociation and filling an oxygen vacancy. Gibbs free energy was calculated at 400 °C. Color code: Fe, purple; Cu, coral; O, red; C, gray; H, white; diffusing-O, green.

partially reduced surface with the existence of metallic Cu nanoparticles on Fe$_3$O$_4$. Furthermore, in situ DRIFTS experiments reveal that surface formate intermediates *only* form on the initial oxidized surface and not on the reconstructed catalyst, which reflects a strong dependence of WGS/RWGS on the specific state of the catalyst surface. The in situ INS spectra after activation under WGS exhibit the presence of surface Cu−H and hydroxyl species, supported by assignments from DFT simulations, but not the vibrations from surface formate species. TPSR experiments also support a redox mechanism because the kinetic evolution of CO$_2$ preceeds that of H$_2$ for WGS over CuCrFeO$_x$, while the evolutions of CO$_2$ and H$_2$ are concurrent for surface formate decomposition that is representative of the associative mechanism. SSITKA experiments (H$_2$^{16}O + C^{16}O ↔ H$_2$^{18}O + C^{16}O) exhibited extensive scrambling of ^{18}O/^{16}O atoms at the surface that is characteristic of a redox mechanism.

DFT calculations found the redox mechanism to be energetically favored over the associative mechanism. The slow step for the associative mechanism is likely the surface HO−CO* coupling (E_{act} = 0.73 eV), whereas the slow step for the redox mechanism is likely the surface CO* oxidation by Fe$_3$O$_4$ lattice O (E_{act} = 0.39 eV). Water dissociation is facile on Fe−O sites near the Cu cluster with little or no barriers. The DFT simulations also show that either mechanism proceeds easily at the Cu−Fe$_3$O$_4$ interface, the catalytic active site for WGS/RWGS.

In summary, a combination of in situ spectroscopic, kinetic, and computational studies was utilized to shed light upon the WGS reaction mechanism, redox versus associative, over the industrial-type CuCrFeO$_x$ catalyst. All the experimental studies and also the DFT calculations support the redox mechanism as

the dominant reaction pathway on the activated CuCrFeO$_x$ catalyst without any supporting evidence found for the associative mechanism.

■ ASSOCIATED CONTENT

ⓈSupporting Information

The Supporting Information is available free of charge on the ACS Publications website at DOI: 10.1021/jacs.9b03516.

SSITKA-reactor scheme, NAP-XPS for RWGS, INS spectra for formic acid, simulated vibrational modes of formic acid, DFT calculations, and SSITKA (PDF)

■ AUTHOR INFORMATION

Corresponding Author
*wuz1@ornl.gov

ORCID ⓞ
Felipe Polo-Garzon: 0000-0002-6507-6183
Victor Fung: 0000-0002-3347-6983
Yu Tang: 0000-0001-9435-9310
Franklin Tao: 0000-0002-4916-6509
Yongqiang Cheng: 0000-0002-3263-4812
Minghui Zhu: 0000-0003-1593-9320
Israel E. Wachs: 0000-0001-5282-128X
De-en Jiang: 0000-0001-5167-0731
Zili Wu: 0000-0002-4468-3240

Present Addresses
▽W. L. Gore and Associates, Newark, DE 19711, United States
○State Key Laboratory of Chemical Engineering, East China University of Science and Technology, Shanghai 200237, P. R. China

■ REFERENCES

(1) Bosch, C.; Wild, W. U.S. Patent 1115776 A, 1914.

(2) Ratnasamy, C.; Wagner, J. P. Water Gas Shift Catalysis. *Catal. Rev.: Sci. Eng.* **2009**, *51* (3), 325−440.

(3) Newsome, D. S. The Water-Gas Shift Reaction. *Catal. Rev.: Sci. Eng.* **1980**, *21* (2), 275−318.

(4) Rhodes, C.; Hutchings, G. J.; Ward, A. M. Water-gas shift reaction: finding the mechanistic boundary. *Catal. Today* **1995**, *23* (1), 43−58.

(5) United States Department of Energy. *The Department of Energy Hydrogen and Fuel Cells Program Plan, DOE/EE-0651*; U. S. Government Printing Office: Washington, DC, 2011.

(6) Zhu, M.; Wachs, I. E. Iron-Based Catalysts for the High-Temperature Water−Gas Shift (HT-WGS) Reaction: A Review. *ACS Catal.* **2016**, *6* (2), 722−732.

(7) Boudjemaa, A.; Daniel, C.; Mirodatos, C.; Trari, M.; Auroux, A.; Bouarab, R. In situ DRIFTS studies of high-temperature water-gas shift reaction on chromium-free iron oxide catalysts. *C. R. Chim.* **2011**, *14* (6), 534−538.

(8) Byron Smith, R. J.; Loganathan, M.; Shantha, M. S. A Review of the Water Gas Shift Reaction Kinetics. *Int. J. Chem. React. Eng.* **2010**, *8*, 1−32.

(9) Khan, A.; Smirniotis, P. G. Relationship between temperature-programmed reduction profile and activity of modified ferrite-based catalysts for WGS reaction. *J. Mol. Catal. A: Chem.* **2008**, *280* (1), 43−51.

(10) Keturakis, C. J.; Zhu, M.; Gibson, E. K.; Daturi, M.; Tao, F.; Frenkel, A. I.; Wachs, I. E. Dynamics of CrO_3−Fe_2O_3 Catalysts during the High-Temperature Water-Gas Shift Reaction: Molecular Structures and Reactivity. *ACS Catal.* **2016**, *6* (7), 4786−4798.

(11) Andreev, A.; Idakiev, V.; Mihajlova, D.; Shopov, D. Iron-based catalysts for the water—gas shift reaction promoted by first-row transition metal oxides. *Appl. Catal.* **1986**, *22* (2), 385−387.

(12) Idakiev, V.; Mihajlova, D.; Kunev, B.; Andreev, A. Effect of copper oxide on the catalytic activity of iron-chromia catalyst for water gas shift reaction. *React. Kinet. Catal. Lett.* **1987**, *33* (1), 119−124.

(13) Zhu, M.; Wachs, I. E. Determining Number of Active Sites and TOF for the High-Temperature Water Gas Shift Reaction by Iron Oxide-Based Catalysts. *ACS Catal.* **2016**, *6* (3), 1764−1767.

(14) Rhodes, C.; Peter Williams, B.; King, F.; Hutchings, G. J. Promotion of Fe_3O_4/Cr_2O_3 high temperature water gas shift catalyst. *Catal. Commun.* **2002**, *3* (8), 381−384.

(15) Rhodes, C.; Hutchings, G. J. Studies of the role of the copper promoter in the iron oxide/chromia high temperature water gas shift catalyst. *Phys. Chem. Chem. Phys.* **2003**, *5* (12), 2719−2723.

(16) Zhu, M.; Rocha, T. C. R.; Lunkenbein, T.; Knop-Gericke, A.; Schlögl, R.; Wachs, I. E. Promotion Mechanisms of Iron Oxide-Based High Temperature Water−Gas Shift Catalysts by Chromium and Copper. *ACS Catal.* **2016**, *6* (7), 4455−4464.

(17) Nguyen, L.; Tao, F. Development of a reaction cell for in-situ/operando studies of surface of a catalyst under a reaction condition and during catalysis. *Rev. Sci. Instrum.* **2016**, *87* (6), 064101.

(18) Kresse, G.; Furthmüller, J. Efficiency of ab-initio total energy calculations for metals and semiconductors using a plane-wave basis set. *Comput. Mater. Sci.* **1996**, *6* (1), 15−50.

(19) Kresse, G.; Furthmuller, J. Efficient iterative schemes for ab initio total-energy calculations using a plane-wave basis set. *Phys. Rev. B: Condens. Matter Mater. Phys.* **1996**, *54* (16), 11169−11186.

(20) Perdew, J. P.; Burke, K.; Ernzerhof, M. Generalized Gradient Approximation Made Simple. *Phys. Rev. Lett.* **1996**, *77* (18), 3865−3868.

(21) Yu, X.; Huo, C.-F.; Li, Y.-W.; Wang, J.; Jiao, H. Fe_3O_4 surface electronic structures and stability from GGA+U. *Surf. Sci.* **2012**, *606* (9), 872−879.

(22) Kresse, G.; Joubert, D. From ultrasoft pseudopotentials to the projector augmented-wave method. *Phys. Rev. B: Condens. Matter Mater. Phys.* **1999**, *59* (3), 1758−1775.

(23) Blochl, P. E. PROJECTOR AUGMENTED-WAVE METHOD. *Phys. Rev. B: Condens. Matter Mater. Phys.* **1994**, *50* (24), 17953−17979.

(24) Monkhorst, H. J.; Pack, J. D. Special points for Brillouin-zone integrations. *Phys. Rev. B* **1976**, *13* (12), 5188−5192.

(25) Henkelman, G.; Uberuaga, B. P.; Jónsson, H. A climbing image nudged elastic band method for finding saddle points and minimum energy paths. *J. Chem. Phys.* **2000**, *113* (22), 9901−9904.

(26) Kappen, P.; Grunwaldt, J.-D.; Hammershøi, B. S.; Tröger, L.; Clausen, B. S. The State of Cu Promoter Atoms in High-Temperature Shift Catalysts—An in Situ Fluorescence XAFS Study. *J. Catal.* **2001**, *198* (1), 56−65.

(27) Grunwaldt, J.-D.; Kappen, P.; Hammershoi, B. S.; Troger, L.; Clausen, B. S. Fluorescence EXAFS for the in situ study on the state of promotors in catalysis. *J. Synchrotron Radiat.* **2001**, *8* (2), 572−574.

(28) Tauster, S. J. Strong metal-support interactions. *Acc. Chem. Res.* **1987**, *20* (11), 389−394.

(29) Mudiyanselage, K.; Senanayake, S. D.; Feria, L.; Kundu, S.; Baber, A. E.; Graciani, J.; Vidal, A. B.; Agnoli, S.; Evans, J.; Chang, R.; Axnanda, S.; Liu, Z.; Sanz, J. F.; Liu, P.; Rodriguez, J. A.; Stacchiola, D. J. Importance of the Metal−Oxide Interface in Catalysis: In Situ Studies of the Water−Gas Shift Reaction by Ambient-Pressure X-ray Photoelectron Spectroscopy. *Angew. Chem., Int. Ed.* **2013**, *52* (19), 5101−5105.

(30) Jacobs, G.; Davis, B. H. In situ DRIFTS investigation of the steam reforming of methanol over Pt/ceria. *Appl. Catal., A* **2005**, *285* (1), 43−49.

(31) Wu, Z.; Li, M.; Overbury, S. H. On the structure dependence of CO oxidation over CeO2 nanocrystals with well-defined surface planes. *J. Catal.* **2012**, *285* (1), 61−73.

(32) Wu, Z.; Li, M.; Mullins, D. R.; Overbury, S. H. Probing the Surface Sites of CeO2 Nanocrystals with Well-Defined Surface Planes via Methanol Adsorption and Desorption. *ACS Catal.* **2012**, *2* (11), 2224−2234.

(33) Busca, G.; Lamotte, J.; Lavalley, J. C.; Lorenzelli, V. FT-IR study of the adsorption and transformation of formaldehyde on oxide surfaces. *J. Am. Chem. Soc.* **1987**, *109* (17), 5197−5202.

(34) Polo-Garzon, F.; Luo, S.; Cheng, Y.; Page, K. L.; Ramirez-Cuesta, A. J.; Britt, P. F.; Wu, Z. Neutron Scattering Investigations of Hydride Species in Heterogeneous Catalysis. *ChemSusChem* **2019**, *12*, 93−103.

(35) Hamilton, N. G.; Warringham, R.; Silverwood, I. P.; Kapitán, J.; Hecht, L.; Webb, P. B.; Tooze, R. P.; Zhou, W.; Frost, C. D.; Parker, S. F.; Lennon, D. The application of inelastic neutron scattering to investigate CO hydrogenation over an iron Fischer−Tropsch synthesis catalyst. *J. Catal.* **2014**, *312*, 221−231.

(36) Zhu, M.; Wachs, I. E. Resolving the Reaction Mechanism for H_2 Formation from High-Temperature Water−Gas Shift by Chromium−Iron Oxide Catalysts. *ACS Catal.* **2016**, *6* (5), 2827−2830.

(37) Gokhale, A. A.; Dumesic, J. A.; Mavrikakis, M. On the Mechanism of Low-Temperature Water Gas Shift Reaction on Copper. *J. Am. Chem. Soc.* **2008**, *130* (4), 1402−1414.

(38) Huang, L.; Han, B.; Zhang, Q.; Fan, M.; Cheng, H. Mechanistic Study on Water Gas Shift Reaction on the Fe_3O_4 (111) Reconstructed Surface. *J. Phys. Chem. C* **2015**, *119* (52), 28934−28945.

(39) Xue, P.; Fu, Z.; Yang, Z. The density functional theory studies on the promoting effect of the Cu-modified Fe_3O_4 catalysts. *Phys. Lett. A* **2015**, *379* (6), 607−612.

(40) Li, X.; Paier, J.; Sauer, J.; Mirabella, F.; Zaki, E.; Ivars-Barceló, F.; Shaikhutdinov, S.; Freund, H. J. Surface Termination of Fe_3O_4(111) Films Studied by CO Adsorption Revisited. *J. Phys. Chem. B* **2018**, *122* (2), 527−533.